Journal of The Electrochemical Society, **155** (5) B449-B454 (2008)
0013-4651/2008/155(5)/B449/6/$23.00 © The Electrochemical Society

Surface Modification of Ni-YSZ Using Niobium Oxide for Sulfur-Tolerant Anodes in Solid Oxide Fuel Cells

Songho Choi, Jenghan Wang,[a] Zhe Cheng,* and Meilin Liu,z**

Center for Innovative Fuel Cell and Battery Technologies, School of Materials Science and Engineering, Georgia Institute of Technology, Atlanta, Georgia 30332, USA

The surface of a dense Ni–yttria-stabilized zirconia (YSZ) anode for solid oxide fuel cells (SOFCs) was modified with niobium oxide (Nb_2O_5) in order to achieve sulfur tolerance. Results suggest that Nb_2O_5 was reduced to NbO_2 under SOFC operating conditions, which has high electrical conductivity and catalytic activity toward hydrogen oxidation. The NbO_x-coated dense Ni-YSZ cermet anode showed sulfur tolerance when exposed to 50 ppm H_2S at 700°C over 12 h. Raman spectroscopy and X-ray diffraction analysis suggest that different phases of niobium sulfides (NbS_x) were formed on the surfaces of niobium oxides. Furthermore, density of state (DOS) analysis of NbO_2, NbS, and NbS_2 indicates that the electronic structure of niobium sulfides are similar to that of NbO_2; they are electrically conductive and catalytically active for hydrogen oxidation in H_2S containing fuels under the conditions studied.
 [DOI: 10.1149/1.2844366]

Manuscript submitted October 12, 2007; revised manuscript received December 20, 2007.
Available electronically March 11, 2008.

The advantages of solid oxide fuel cells (SOFCs) over other types of fuel cells include high energy efficiency and excellent fuel flexibility.[1,2] In particular, the possibility of direct utilization of fossil fuels and renewable fuels (e.g., biofuels) may significantly reduce the cost of SOFC technologies. However, it is known that these types of fuels contain many contaminants that may be detrimental to SOFC performance. For example, sulfur could deteriorate the functionality of Ni-based anodes under SOFC operating conditions.[3] Even though the desulfurization of fuels for the removal of sulfur species in some levels is available, the process becomes another source of high cost and system complexity in order to achieve low concentration of sulfur species. Thus, the design of sulfur-tolerant anode materials is essential to durability and commercialization of SOFCs.

Investigations into the mechanism of sulfur poisoning suggest[4-6] that the performance degradation of a Ni–yttria-stabilized zirconia (YSZ) anode can be attributed to sulfur adsorption on active surface sites and subsequent formation of two-dimensional (2D) surface nickel sulfides upon exposure to H_2S. The degree of the degradation in anode performance varies with operating conditions such as temperature, concentration of H_2S, and current density passing through the cell.[4,7] Although several alternative anode materials, such as $La_{1-x}Sr_xVO_3$,[8] $La_{1-x}Sr_xTiO_3$,[9] Y-doped $SrTiO_3$,[10] and CeO_2-based anodes,[11,12] have shown some sulfur tolerance, none of these materials can satisfy all the practical requirements for SOFCs. For example, reasonable sulfur tolerance was observed with titanium oxide– and vanadium oxide–based anodes, but their electrochemical performances are relatively low. In the case of $Cu/CeO_2/YSZ$, tolerance to sulfur poisoning was observed up to 450 ppm H_2S; however, ion impregnation must be used in the fabrication of the anode and thermal stability of copper should be taken into account. Recently, we studied the effect of surface modification[13] of Ni-YSZ anodes with Nb_2O_5 coating on sulfur tolerance.

In this paper, we report our findings in surface modification of Ni-YSZ using niobium oxide for sulfur tolerance. In order to minimize experimental uncertainty in porous anodes, a dense Ni-YSZ anode was used for this study. Sulfur tolerance of Ni-YSZ coated with a thin film of niobium oxide was investigated experimentally and computationally in order to understand the mechanism of sulfur tolerance.

Experimental

Phase analysis and electrical property of reduced Nb_2O_5.— To investigate the phase stability of Nb_2O_5 under operating conditions of the anode, reduced powder was prepared by reducing Nb_2O_5 powder in H_2 (UHP grade, Airgas) at 750°C for 24 h, and the resulting phase was confirmed as NbO_2 using X-ray diffraction (XRD) (Philips, PW-1800). The electrical conductivity of the reduced phase was measured using impedance spectroscopy in a two-electrode configuration in the temperature range from 600 to 850°C with 50°C increments in H_2 after a Nb_2O_5 pellet sintered at 1250°C for 5 h was reduced under the same condition. A porous Pt cathode was formed on the other side of the electrolyte by brush painting and subsequent firing at 850°C for 3 h of Pt paste (Heraeus). The impedance system consisting of a potentiostat/galvanostat (EG&G, 273A) and a lock-in amplifier (Princeton Applied Research) interfaced with a computer was used.

Preparation of dense Ni-YSZ and surface modification with Nb_2O_5.— As shown in Fig. 1, two-layered cells consisting of dense YSZ (Tosoh) and Ni-YSZ were prepared using a copressing and cosintering method in 4% H_2 balanced with Ar at 1400°C for 3 h. The thicknesses of the YSZ (8 mol % Y-doped zirconia) electrolyte and the Ni-YSZ anode were about 400 and 100 μm, respectively. For the dense Ni-YSZ anode, 20 wt % of metal Ni powder (Alfa Asear, 3–5 μm) was used to avoid significant distortion of the cells due to mismatch of the coefficient of thermal expansion. The surface of dense Ni-YSZ was confirmed to be conductive using an ohmmeter with a well-distributed Ni network in the dense structure. Reactive sputtering was used to deposit a ~500 nm thick Nb_2O_5 layer on the top of the dense Ni-YSZ surface. A small area on the edge of the

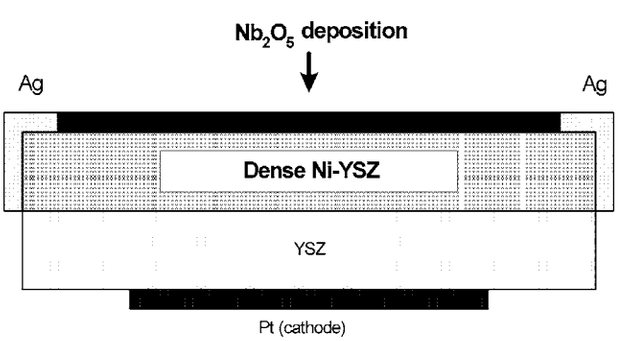

Figure 1. Schematic of dense Ni-YSZ structure with Nb_2O_5 coating for sulfur tolerance test.

* Electrochemical Society Student Member.
** Electrochemical Society Active Member.
[a] Present address: Department of Applied Chemistry and Center for Interdisciplinary Molecular Science, National Chiao Tung University, Hsinchu, 30010, Taiwan.
[z] E-mail: meilin.liu@mse.gatech.edu

dense Ni-YSZ layer was masked for current collection as shown in Fig. 1. A Ag current collector was used and directly contacted with Ni-YSZ through the masked area in order to reduce any contribution between the current collector and the modified surface with Nb_2O_5 coating.

Electrochemical characterization and sulfur poisoning test.— The electrochemical behavior of functional cells of Pt/YSZ/dense Ni-YSZ with Nb_2O_5 coating was characterized by measuring peak power density and impedance spectra. The impedance was typically measured in the frequency range of 1 MHz to 0.01 Hz using a lock-in amplifier (Princeton Applied Research) and a potentiostat/galvanostat (EG&G, 273A) interfaced with a computer. The fuel cell performance was acquired using the CorrWare software. For sulfur poisoning tests, the anode was exposed to H_2 containing 50 ppm H_2S at a flow rate of 40 mL/min while the cathode was exposed to ambient air. The experimental apparatus was as described elsewhere.[4] The sulfur tolerance tests were conducted in a potentiostatic mode, i.e., monitoring the cell current at a constant cell voltage, as the fuel was switched from H_2 to 50 ppm H_2S containing fuel or vice versa. Each cell was tested in clean H_2 at 700°C for several days until the performance was stabilized before a small amount of H_2S was introduced.

Surface analysis.— To investigate the surface change in a H_2S containing fuel, fine Nb_2O_5 powder with a large surface area was prepared by evaporating the solution of $Nb(HC_2O_4)_4{\cdot}6H_2O$ at 150°C. The collected powder was calcinated at 500°C for 5 h and reduced in dry H_2 at 800°C for 24 h. Then, the powder was exposed to 100 ppm H_2S balanced with H_2 at 700°C for 15 h. The reaction chamber was cooled down in Ar, instead of 100 ppm H_2S, to avoid further reaction of the powder with H_2S at lower temperatures. The powder samples were examined using Raman microspectroscopy (Renishaw 2000, 514 nm laser, 1 mW) and XRD before and after exposure to 100 ppm H_2S, and after regeneration in clean H_2.

Computational

The Vienna Ab Initio Simulation Package (VASP),[14-16] at the density functional theory (DFT) level with periodic conditions, was used for the quantum-chemical calculations.

Electronic structure calculations.— The generalized gradient approximation[17] with the Perdew-Wang 1991 (PW91) exchange-correlation functional[18] and the projector-augmented wave method,[19,20] a method combining the accuracy of augmented plane waves with the cost-effective pseudopotentials implemented in VASP, was applied. This plane wave expansion included all plane waves with their kinetic energies smaller than the chosen cutoff energy of 400 eV to ensure the convergence with respect to the basis set and the efficiency of the computational cost. The Brillouin-zone (BZ) integration was sampled with $0.05 \times 2\pi$ (1/Å) spacing in reciprocal space by the Monkhorst–Pack scheme.[21] The crystal structures of the interest oxides and sulfides were initially optimized and compared to XRD observations to validate the computational methodology. On the basis of optimized structures, the density of state (DOS) calculations were performed for electronic structure study.

Phase diagram calculations.— To take into consideration of the environmental effects under the condition for fuel cell operation, the Gibbs free energy $G(T,p)$ of the whole system was calculated as a function of temperature and pressure from the DFT results, as described elsewhere.[22-26] The Gibbs free energy for a solid phase was approximated by the DFT computed energy, $G_{\text{surface}}(T,p) \approx E^{\text{DFT}}_{\text{surface}}$ because of the relatively small variation, <10 meV, in a wide range of temperatures (<1500 K) and pressures (<100 atm).[22,26] The Gibbs free energy of the gas phase O_2 was obtained by adding the thermodynamic corrections from the database[27] to the DFT values: $G_{O_2}(T,p) = E^{\text{DFT}}_{O_2} + \Delta H_{O_2}(T,p^0) + RT\ln(p_{O_2}/p^0)$, where H_{O_2} is the standard enthalpy of O_2 molecule and R is the gas constant.

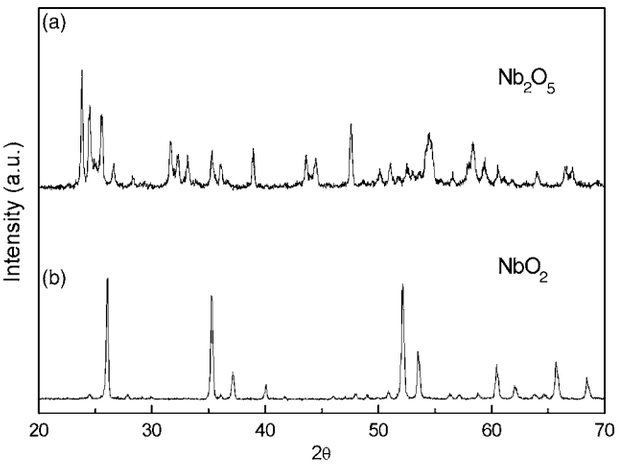

Figure 2. XRD spectra of Nb_2O_5 power (a) before and (b) after reduction in dry H_2 at 750°C for 24 h.

Vibrational analysis.— The crystal phonons were computed from the optimized geometries by applying the finite displacement approach.[28,29] The interatomic force-constant matrix (Hessian matrix) was derived from a set of calculations on a periodically repeated super cell that contains several unit cells. At the starting point, all atoms were put at the equilibrium position. Then each atom was slightly displaced and the forces on all atoms were calculated. These computed forces were proportional to the interatomic force constants times the displacement. The full Hessian matrix was obtained by considering all symmetry-inequivalent displacements and truncated due to the finite size of the super cell as it rapidly decayed to zero with increasing interatomic separations. The frequencies as a function of the normal modes were obtained via matrix diagonalization and computed at the Γ-point of the BZ in order to allow comparison to the spectroscopic observations.

Results and Discussion

Phase analysis of Nb_2O_5 under reducing conditions.— As shown in Fig. 2, Nb_2O_5 was reduced to NbO_2 after being immersed in dry H_2 at 750°C for one day. Thus, Nb_2O_5 is not stable under fuel cell operating conditions, and the actual phase will be either Nb_2O_5 or NbO_2, depending on the partial pressure of oxygen. It is known that the reduced phases of Nb_2O_5 have high electrical conductivities while their ionic conductivities are negligible.[30,31] To determine the temperature dependence of electrical property of NbO_2, we measured the electrical conductivity of NbO_2 in pure H_2. As shown in Fig. 3, NbO_2 displayed typical metallic behaviors.

The result of NbO_2 formation was also confirmed with the predicted phase diagram from Gibbs free energy calculations, as shown in Fig. 4. For pressure effect, the oxygen-rich oxides appear in the higher oxygen partial pressures. For the temperature effect, the oxidized phases are more stable at low temperatures because the oxidation processes are all exothermic: $Nb + \frac{1}{2}O_2 \rightarrow NbO$, $\Delta E = -4.26$ eV; $NbO + \frac{1}{2}O_2 \rightarrow NbO_2$, $\Delta E = -3.74$ eV; and $NbO_2 + \frac{1}{2}O_2 \rightarrow \frac{1}{2}Nb_2O_5$, $\Delta E = -1.70$ eV. Under the experimental condition at 750°C, the Nb_2O_5 will reduce to NbO_2 when $p_{O_2} < 10^{-22}$ atm at thermoequilibrium. In addition, the observed electrical behavior of NbO_2 is consistent with the prediction from the DOS analysis; as shown in Fig. 5, only Nb_2O_5 in the Nb–O systems is an insulator and has a wide bandgap around the Fermi level.

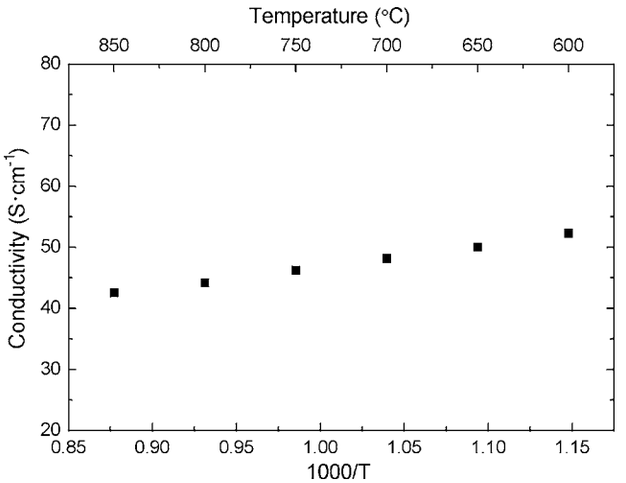

Figure 3. Conductivity of NbO_2 reduced from Nb_2O_5 as a function of temperature in dry H_2 measured by two-electrode ac measurement.

Effect of Nb_2O_5 coating on electrochemical performances.— Shown in Fig. 6a are the power densities as a function of current density for cells of Pt/YSZ/dense Ni-YSZ with and without Nb_2O_5 coating in dry H_2 at 700°C. The peak power density was ~23 mW/cm^2 for the cell without Nb_2O_5 coating and ~49 mW/cm^2 for the cell with Nb_2O_5 coating on the dense Ni-YSZ anode. This enhancement in power output resulted from the reduced NbO_2 with high electrical conductivity under operating conditions; the conductive NbO_2 coatings may create additional triple phase boundaries for the electrochemical reactions. In addition, the good catalytic activity of niobium oxides for H_2 dissociative adsorption claimed by previous studies[31-33] may also attribute to the enhanced power density of Nb_2O_5 modified Ni-YSZ anode.

Shown in Fig. 6b are the impedance spectra of the two cells under open-circuit conditions. The observed increase in power density was due mainly to the decrease in the interfacial polarization resistance from about 15 to 7 Ω cm^2, which may be attributable to the improved catalytic activity of NbO_2 or the increased triple-phase boundary length due to the addition of NbO_2 to the dense Ni-YSZ anode.

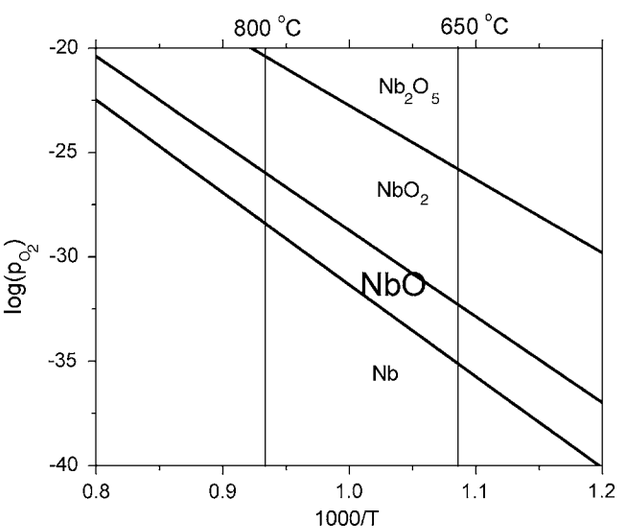

Figure 4. Phase diagram of the Nb-O system.

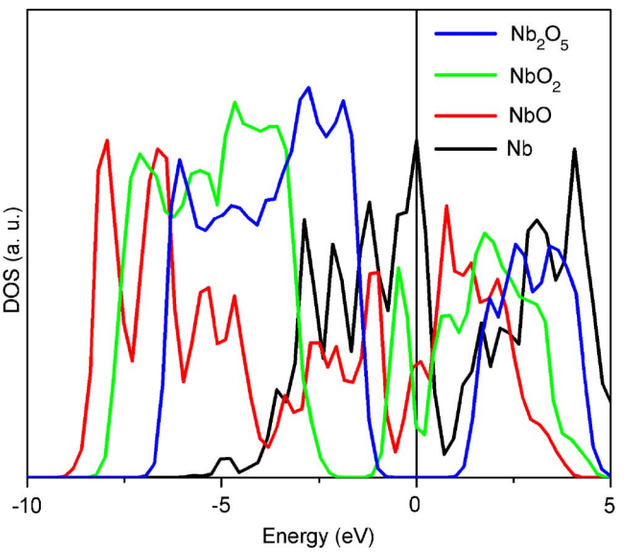

Figure 5. (Color online) Total DOS of Nb_2O_5, NbO_2, NbO, and Nb.

Sulfur tolerance test.— Shown in Fig. 7 is the sulfur tolerance test of Pt/YSZ/dense Ni-YSZ with Nb_2O_5 coating. The Nb_2O_5-coated Ni - YSZ anode was exposed to 50 ppm H_2S after the cell performance was stabilized in H_2 at 700°C. The operating temperature was kept at 700°C to observe a significant sulfur-poisoning effect. The change of current density as a function of time by switching the fuel from H_2 to 50 ppm H_2S balanced with H_2 shows a slight, quick drop when H_2S is introduced, but, immedi-

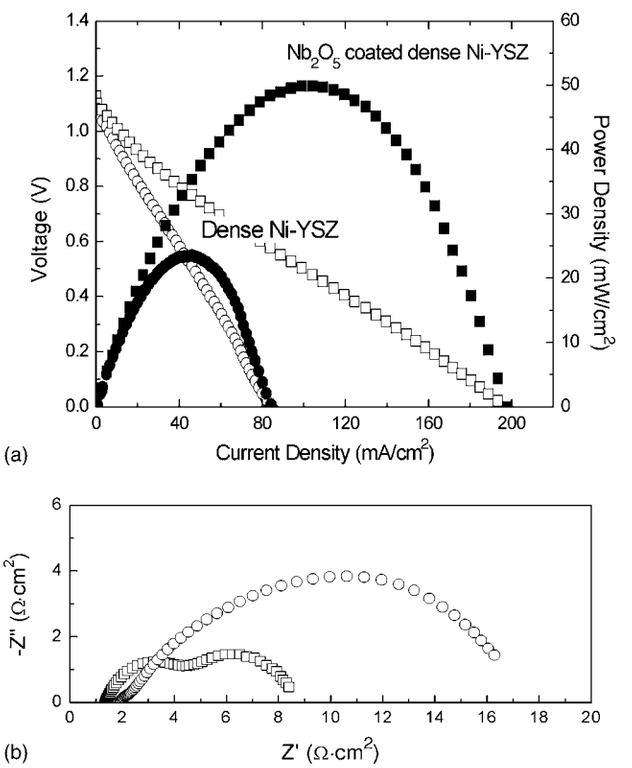

Figure 6. Comparison of (a) power densities as a function of current densities and (b) impedance spectra of Pt/YSZ/dense Ni-YSZ with (squares) and without (circles) Nb_2O_5 coating in dry H_2 at 700°C.

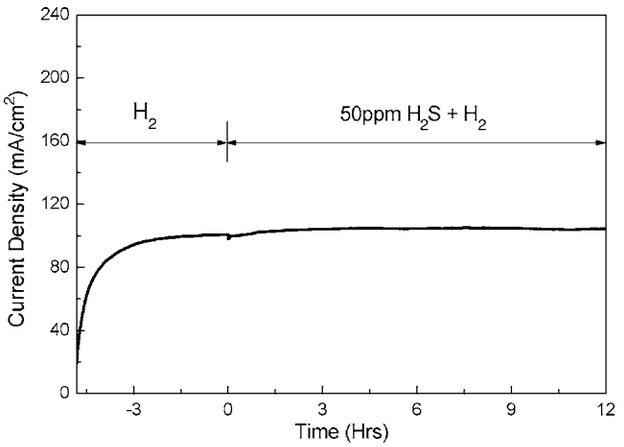

Figure 7. Change of current density as a function of time of Pt/YSZ/dense Ni-YSZ with Nb_2O_5 deposition in dry H_2 and 50 ppm H_2S balanced with H_2 at 700°C after 0.5 V is applied.

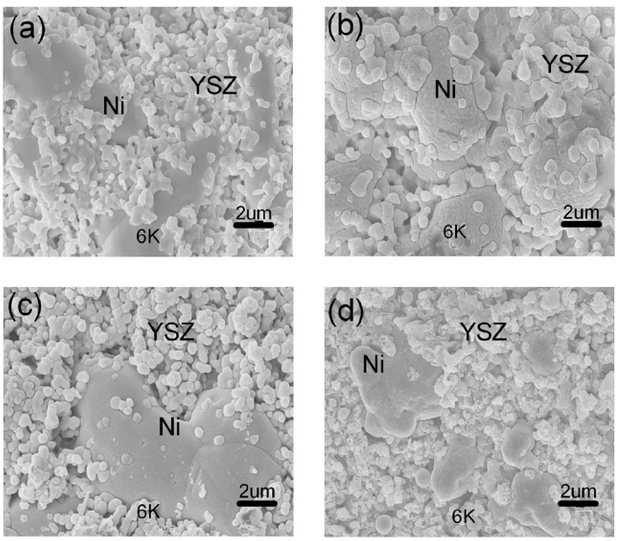

Figure 8. SEM analysis of dense Ni-YSZ surfaces (a) before and (b) after Nb_2O_5 coating, and of Nb_2O_5 coated Ni-YSZ (c) after annealing in H_2 at 700°C and (d) after sulfur tolerance tests in 50 ppm H_2S balanced with H_2 at 700°C over 15 h, respectively.

ately, the current density increased slightly above the initial current density in H_2 during the exposure in 50 ppm H_2S, followed by stable performance over 12 h. There is a slight increase of current density in 50 ppm H_2S, and it is achieved over ~3 h. This behavior is not well explained with the given data. However, the result shows that the modified anode surface has excellent sulfur tolerance, which might correspond to the good catalytic activity for H_2S and H_2 oxidation of the surface sulfides formed on the surface of NbO_2 in low concentration of H_2S. It is apparent that the gain of current density in H_2S is attributable to the chemical surface change of NbO_2 because it is not shown in the Ni-YSZ anode without surface modification. The initial slight drop of the current density as H_2S is introduced may be affected by the sulfur adsorption on active sites composed of Ni and YSZ.

SEM and EDS analysis.— After the anode with Nb_2O_5 coating was exposed to a hydrogen fuel containing 50 ppm H_2S, the surface morphology and the chemical composition of the anode surfaces were investigated using scanning electron microscopy (SEM) and energy-dispersive spectroscopy (EDS) as shown in Fig. 8 and 9, respectively. For comparison, the surfaces with Nb_2O_5 coating without (b) and with (c) annealing in H_2 are also shown in Fig. 8. It is seen in Fig. 8c that the surface was covered with Nb_2O_5 coating, and it appears that the coating layer became thin and dense after annealing in H_2, as expected from the reduction of Nb_2O_5 to NbO_2. The surface morphology appeared to change after sulfur tolerance tests, as shown in Fig. 8d, compared to the surface before the deposition, shown in Fig. 8a and c. From EDS analysis for the surface after the sulfur-poisoning test, as shown in Fig. 9, Nb was detected on both the Ni and YSZ surfaces, indicating that the whole surface was modified and Ni surface modification with Nb_2O_5 was maintained. However, elemental sulfur, which was expected after H_2S exposure, was not detected using EDS.

Surface analysis.— To further study the surface change of the anode in H_2S exposure, surfaces of NbO_2 powder before, after the exposure to 100 ppm H_2S balanced with H_2 at 700°C for 15 h, and after regeneration in H_2 were analyzed using Raman spectroscopy, as shown in Fig. 10. Several sharp peaks (indicated by an asterisk in Fig. 10b) appeared after being exposed to 100 ppm H_2S compared to the spectrum of NbO_2 in Fig. 10a. These Raman peaks, assigned from the DFT calculation and compared to previous works in Table I,[34-36] resulted from the 3*R*-NbS_2 formation. The high-frequency vibration at 463 cm^{-1} and the low-frequency vibrations at 187 and 155 cm^{-1} can be attributed to NbS_2 formation as compared in Table I. The peaks at 393 and 347 cm^{-1}, for A_1 and E vibrational modes, respectively, may be identified as the 3*R*-NbS_2 crystal phonons but the identification is not positive, as these peaks overlap the peaks of NbO_2 at 403 and 344 cm^{-1}. Interestingly, the new peaks disappeared after exposing the to H_2 for 12 h, indicating that the new phase was decomposed as shown in Fig. 10c.

Furthermore, the sulfide phase formed in 100 ppm H_2S exposure was also analyzed by XRD, as shown in Fig. 11. Several new peaks were found and identified as $Nb_{0.9}S$ after exposure. In addition, some nonstoichiometric phases could be expected due to the broadness of the peaks.

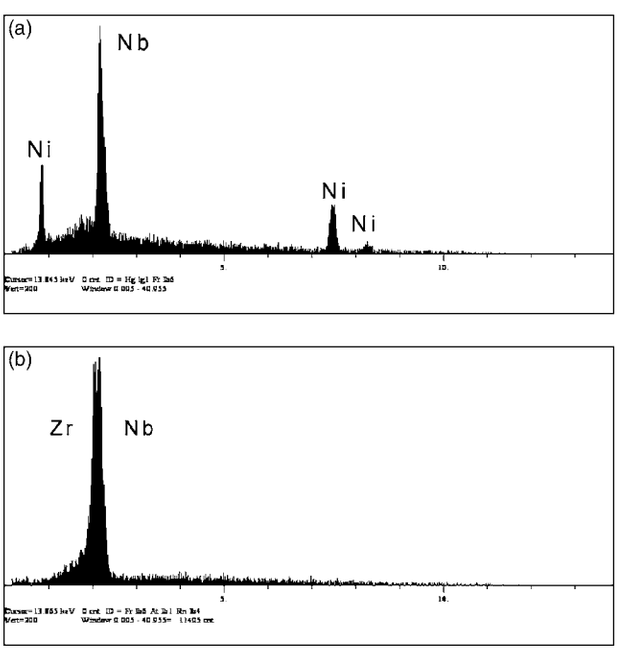

Figure 9. EDS spectra from (a) Ni surface and (b) YSZ surface of dense Ni-YSZ coated with Nb_2O_5 after sulfur tolerance test in 50 ppm H_2S balanced with H_2 at 700°C over 15 h.

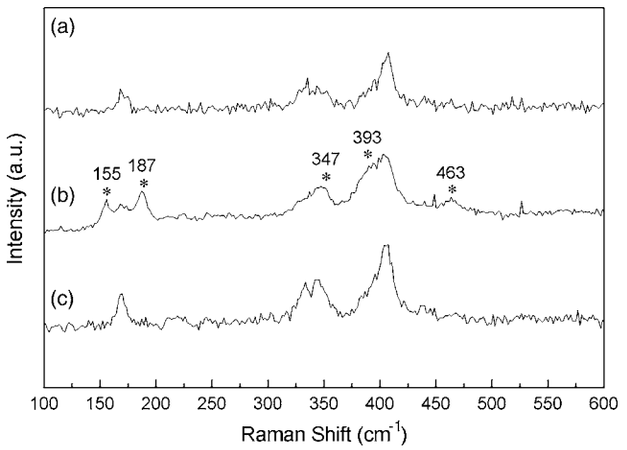

Figure 10. Raman spectra of (a) Nb_2O_2 powder after reduction in H_2 at 800°C for 24 h, (b) NbO_2 powder after being exposed to 100 ppm H_2S balanced with H_2 at 700°C for 15 h, and (c) Nb_2O_5 powder after regeneration in H_2 at 700°C for 15 h.

The different phases observed from Raman (NbS_2) and XRD ($Nb_{0.9}S$) spectroscopy can be attributed to the detection limits between them. Raman spectroscopy is more sensitive to the surface phases because of the limited penetration depth of visible light, while XRD has much greater penetration depth, probing the bulk properties. As a result, the sulfur-rich compound (NbS_2), detected from Raman spectroscopy, is expected to appear in the top layers when H_2S directly reacts with the surface. The deeper layers, detected by XRD, have a Nb-rich stoichiometry because the formation depends on the bulk diffusion of sulfur atoms. In both cases, niobium sulfides were formed by the reaction of NbO_2 with H_2S on the surface. However, in the functional cell tests, no evidence of sulfide formation was identified from the modified anode surface after exposure to 50 ppm H_2S, probably due to the oxidative environment in the presence of water and oxygen ions transferred from the electrolyte in a functional cell.

Table I. Experimentally observed and computed Raman frequencies of NbS_2.

	Modes	Expt.	Calc.	Ref.
		463		458,[23] 462[24]
	A_1	393	394	382[22], 386[23,24]
NbS_2	E	347	349	329,[22] 330,[23] 322[24]
		187		191[24]
		155		150,[22] 158[23]

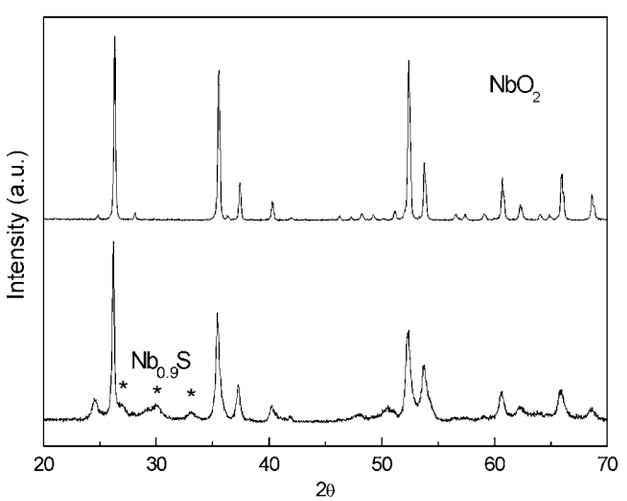

Figure 11. XRD spectra of (a) NbO_2 powder after reduction in H_2 at 800°C for 24 h and (b) NbO_2 powder after being exposed to 100 ppm H_2S balanced with H_2 at 700°C for 15 h.

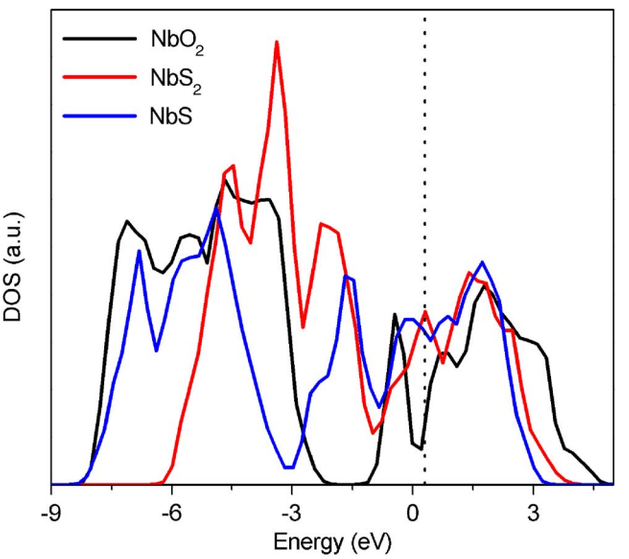

Figure 12. (Color online) DOS analysis of before (NbO_2) and after (NbS_2) sulfur exposure.

DOS analysis.— The degradation of the electrochemical performance corresponds to the changes of conductivity and catalytic ability of the anode materials when sulfides are formed in the sulfur-poisoning process. The conductivity can be attributed to the bandgap calculations, and the catalytic ability of H_2 oxidation corresponds to the band structure of the materials. These intrinsic properties can be understood from the electronic structure (DOS) analysis. Shown in Fig. 12 is the DOS analysis of the NbO_2 (before H_2S exposure) and the possible sulfides, NbS and NbS_2 (after H_2S exposure). The results show that no obvious bandgaps were found around the Fermi level in the sulfides, indicating that the sulfide-covered anode is still conductive for the electrochemical reactions. In addition, comparing the DOS of the phases without (NbO_2) and with sulfur exposure (NbS and NbS_2), all of them have similar DOS distribution, indicating that the catalytic activity of the sulfides is as good as that of NbO_2. Thus, the DOS analysis predicts that both NbO_2 and niobium sulfides (NbS and NbS_2) are conductivity and catalytically active.

Surface regeneration.— To investigate the regeneration process on the modified anode with Nb_2O_5, the current density was monitored in a short-term test carried out at 700°C with fuel transitions, from H_2 to 50 ppm H_2S with H_2 and vice versa, as shown in Fig. 13. After the sulfur tolerance test with 50 ppm H_2S, the fuel was switched back to pure H_2 and the current density was restored to the initial value in the measurement. Similar to the result in the sulfur tolerance test in Fig. 7, the current density in Fig. 13 shows a quick drop when H_2S is introduced and slowly increased over the following 3 h. Furthermore, in the regeneration process when 50 ppm H_2S was switched to pure H_2, the current density increased abruptly and started to decrease slowly, followed by stable current density. The initial drop in H_2S may be attributable to the sulfur adsorption on the Ni surfaces that are not covered by NbO_2. The abrupt increase in the regeneration process with H_2 reintroduction could be considered as the desorption of the adsorbed sulfur. The slow increase of current density in 50 ppm H_2S and slow decrease in pure H_2 can be explained by the surface changes, the formation of niobium sulfides,

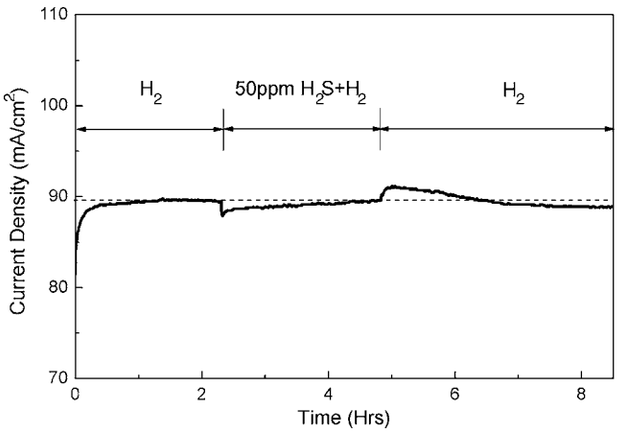

Figure 13. Variation of current density depending on fuels of Pt/YSZ/dense Ni-YSZ with Nb_2O_5 coating in dry H_2 and 50 ppm H_2S balanced with H_2 at 700°C after 0.5 V is applied.

of NbO_2 on Ni-YSZ by the interaction with H_2S, as identified in Raman spectroscopy and XRD. The formation and decomposition of niobium sulfides can be taken into account for the slow changes. This behavior is not seen in the conventional Ni-YSZ anode, indicating that the changes of current density in H_2S can be attributed to the surface modification with Nb_2O_5.

Conclusions

We have demonstrated the possibility of surface modification for sulfur tolerance using a dense Ni-YSZ anode coated with a layer of niobium oxide. The increase in peak power density for a cell with a surface modified dense Ni-YSZ anode was due mainly to the decrease in the interfacial polarization resistance originating in the niobium oxide coating. It was found that Nb_2O_5 was reduced to NbO_2 on exposure to H_2, as predicted from the computed phase diagram. The metallic behavior of NbO_2 was confirmed by both conductivity measurement and theoretical calculation.

In the sulfur tolerance test, the cell current remained relatively constant on exposure to 50 ppm H_2S for over 12 h. The observed excellent sulfur tolerance of a Nb_2O_5–coated Ni-YSZ anode is attributed to the good catalytic activity for H_2 oxidation of the surface sulfides formed on the niobium oxide surface in low concentrations of H_2S.

Furthermore, the observed slow changes in cell current as the fuel was switched from clean H_2 to H_2 containing 50 ppm H_2S (or vice versa) can be explained by the corresponding phase changes of the niobium oxide on Ni-YSZ, as identified using Raman spectroscopy and XRD analyses. The formation and decomposition of niobium sulfides can be taken into account for the slow changes and correspond to the Raman spectrum change before and after H_2S exposure. However, in the functional cell tests, no evidence of sulfide formation was observed after the exposure to 50 ppm H_2S, due probably to limited sulfide formation because of the inflow of oxygen ions from the cathode under active fuel cell operation.

Acknowledgments

This work was supported by the U.S. DOE SECA Core Technology Program (grant no. DE-FC26-04NT42219) and the DOE Office of Basic Energy Sciences, Catalysis Science Program (grant no. DE-FG02-06ER15837).

Georgia Institute of Technology assisted in meeting the publication costs of this article.

References

1. B. C. H. Steeele and A. Heinzel, *Nature (London)*, **414**, 345 (2001).
2. A. Atkinson, S. Barnett, R. J. Gorte, J. T. S. Irivine, A. J. McEvoy, M. Morgensen, S. C. Singhal, and J. Vohs, *Nat. Mater.*, **3**, 17 (2004).
3. M. Gong, X. Liu, J. Trembly, and G. Johnson, *J. Power Sources*, **168**, 289 (2007).
4. S. Zha, Z. Cheng, and M. Liu, *J. Electrochem. Soc.*, **154**, B201 (2007).
5. Z. Cheng and M. Liu, *Solid State Ionics*, **178**, 925 (2007).
6. Y. M. Choi, C. Compson, M. C. Lin, and M. Liu, *Chem. Phys. Lett.*, **421**, 179 (2006).
7. Y. Matsuzaki and I. Yasuda, *Solid State Ionics*, **132**, 261 (2000).
8. L. Aguilar, S. Zha, Z. Cheng, J. Winnick, and M. Liu, *J. Power Sources*, **135**, 17 (2004).
9. R. Mukundan, E. L. Brosha, and F. H. Garzon, *Electrochem. Solid-State Lett.*, **7**, A5 (2004).
10. H. Kurokawa, L. Yang, C. P. Jacobson, L. C. D. Jonghe, and S. J. Visco, *J. Power Sources*, **164**, 510 (2007).
11. H. Kim, J. M. Vohs, and R. J. Gorte, *Chem. Commun. (Cambridge)*, **2001**, 2334.
12. H. He, R. J. Gorte, and J. M. Vohs, *Electrochem. Solid-State Lett.*, **8**, A279 (2005).
13. A. Isenberg, U.S. Pat. 4,812,329 (1987).
14. G. Kresse and J. Furthmüller, *Comput. Mater. Sci.*, **6**, 15 (1996).
15. G. Kresse and J. Furthmüller, *Phys. Rev. B*, **54**, 11169 (1996).
16. G. Kresse and J. Hafner, *Phys. Rev. B*, **47**, 558 (1993).
17. C. Lee, W. Yang, and R. G. Parr, *Phys. Rev. B*, **37**, 785 (1988).
18. J. P. Perdew and J. A. Chevary, S. H. Vosko, K. A. Jackson, M. R. Pederson, D. J. Singh, and C. Fiolhais, *Phys. Rev. B*, **46**(11), 6671 (1992).
19. P. E. Blöchl, *Phys. Rev. B*, **50**, 17953 (1994).
20. G. Kresse and D. Joubert, *Phys. Rev. B*, **59**, 1758 (1999).
21. H. J. Monkhorst and J. D. Pack, *Phys. Rev. B*, **13**, 5188 (1976).
22. J. Xie, S. d. Gironcoli, S. Baroni, and M. Scheffler, *Phys. Rev. B*, **59**, 970 (1999).
23. S. Cristol, J. F. Paul, E. Payen, D. Bougeard, S. Clemendot, and F. Hutschka, *J. Phys. Chem. B*, **106**, 5659 (2002).
24. W.-X. Li, C. Stampfl, and M. Scheffler, *Phys. Rev. B*, **68**, 165412 (2003).
25. A. Michaelides, M.-L. Bocquet, P. Sautet, A. Alavi, and D. A. King, *Chem. Phys. Lett.*, **367**, 344 (2003).
26. K. Reuter and M. Scheffler, *Phys. Rev. B*, **65**, 035406 (2001).
27. http://webbook.nist.gov/
28. X. Gonze, *Phys. Rev. B*, **55**, 10337 (1997).
29. G. Kresse, J. Furthmuller, and J. Hafner, *Europhys. Lett.*, **32**, 729 (1995).
30. R. Elo, R. A. Swalin, and W. K. Chen, *J. Phys. Chem. Solids*, **28**, 1625 (1967).
31. C. M. Reich, A. Kaiser, and J. T. S. Irvine, *Fuel Cells*, **1**, 249 (2001).
32. A. Borgschulte, J. H. Rector, B. Dam, R. Griessen, and A. Zuttel, *J. Catal.*, **235**(2), 353 (2005).
33. G. Barkhordarian, T. Klassen, and R. Bormann, *Scr. Mater.*, **49**, 213 (2003).
34. M. Hangyo, K. Kisoda, S. Nakashima, A. Meerschaut, and J. Rouxel, *Physica B*, **219-220**, 481 (1996).
35. W. G. McMullan and J. C. Irwin, *Solid State Commun.*, **45**, 557 (1983).
36. C. J. Carmalt, E. S. Peters, I. P. Parkin, T. D. Manning, and A. L. Hector, *Eur. J. Inorg. Chem.*, **2004**, 4470.